



Trans. Nonferrous Met. Soc. China 33(2023) 3699-3711

Transactions of Nonferrous Metals Society of China

www.tnmsc.cn



Microstructural evolution and mechanical properties of high-temperature pack rolled TiB_w/TA15 composite sheets with network structure

Jian-hang QIAN¹, Ke-huan WANG¹, Yuan-song ZENG², Ming-jie FU², Fu-xin WANG², Gang LIU¹

School of Materials Science and Engineering, Harbin Institute of Technology, Harbin 150001, China;
AVIC Manufacturing Technology Institute, Beijing 100024, China

Received 14 November 2022; accepted 16 May 2023

Abstract: Two TiB_w/TA15-based titanium matrix composites (TMCs) sheets with network structures were rolled at 1000 and 1100 °C with reduction rates of 86.7% (932 mm \times 393 mm) and 89.3% (987 mm \times 461 mm), respectively. The microstructures of the two sheets differed remarkably. The network structure was transformed into a layered structure with disk-like units after rolling. The room-temperature tensile strengths of the sheets rolled at 1000 and 1100 °C were increased by 26.4% (1398 MPa) and 23.0% (1360 MPa), respectively, compared with that of the slab. The tensile strengths of the slab and sheets tested at 600 °C were 561 (slab), 662 (sheet rolled at 1000 °C), and 758 MPa (sheet rolled at 1100 °C). The tensile strength at 650 °C of the sheet rolled at 1100 °C (553 MPa) was the highest.

Key words: titanium matrix composites; network structure; hot rolling; thin sheet; mechanical properties; fracture analysis

1 Introduction

Titanium matrix composites (TMCs) have extremely high specific strengths, elevated elastic moduli, and exceptional thermal durability properties than their unreinforced counterparts [1–4]. Among various TMCs, in-situ synthesized discontinuously reinforced TMCs (DRTMCs) have been extensively reported owing to their isotropic features, secondary formability, better combination properties, and simple fabrication procedures [5]. To further enhance the performance, the distribution of reinforcements within DRTMCs based on Hashin-Shtrikman (H-S) theorem has been investigated [6,7]. HUANG et al [8,9] developed DRTMCs with reinforcement phase network distribution prepared by in-situ reaction hot pressing technique. The resulting DRTMCs with network structure exhibited a superior strength performance than the homogeneously reinforced DRTMCs [10–12].

Numerous thermo-mechanical techniques have been used to improve mechanical properties of DRTMCs with network structure. Related processes include hot forging [13,14], hot extrusion [12,15,16], and hot rolling [17]. ZHANG et al [18] examined the forging processes of TMCs with network structure and noticed an improvement in the strength and elongation of TMCs. FENG et al [19,20] noticed that the orientations of TiB whiskers became uniform after hot extrusion, which is suitable for the effective strengthening of DRTMCs. Meanwhile, high temperatures can be used for heat treatment of DRTMCs since the pinning effect of TiB_w can inhibit the growth of grains [21]. WANG et al [22] observed the preferable distribution of TiB whiskers along the rolling direction (RD), resulting in sheets with a better plasticity.

In the hot rolling process, the high temperature condition reduces the difficulty of plastic deformation of the materials, allowing for a larger deformation per pass, and improving production efficiency [23]. At the same time, due to the effect of temperature, the changes in the material structure are more active [24]. Due to the high deformation resistance of titanium-based composites, the sheet metal needs to be prepared by hot rolling process [25].

The preparation of thin sheets is the foundation for forming thin-walled components. However, the difficulty in preparing large-sized thin sheets has resulted in rare application of titanium-based composite thin-walled components. To address this issue, we investigated the process of preparing large-sized thin sheets through the pack hot rolling method at the temperature near the phase transformation point. The results confirm the feasibility of using this method to prepare large-sized thin sheets, which has significant implications for the industrial application of this material. Furthermore, the results indicate that thin sheet materials exhibit excellent strength properties. Fracture analysis explains the impact of experimental conditions on the mechanical properties.

2 Experimental

The material consisted of TiB_w/TA15-based DRTMCs with network structure, with the content of TiB fixed at 3.5 vol.%. DRTMCs were produced by vacuum hot-press sintering method. During the fabrication, large-sized spherical TA15 alloy powders (Ti-6.5Al-2Zr-1Mo-1V; size: 75-150 μm) and fine TiB₂ powders (size: 1-3 μm) were used as raw materials. All powders were ball-milled in a planetary ball-milling machine with a relatively low

energy for 8 h under argon protective atmosphere. Subsequently, the mixed powders were added to the sintering furnace and heated to 1300 °C under vacuum conditions. The reaction between TiB₂ and Ti in TA15 powder can be described by Reaction (1):

$$Ti(s)+TiB_2(s)=2TiB(s)$$
 (1)

After hot sintering, TiB whiskers were mainly formed near the boundaries of TA15 particles [26]. The scanning electron microscopy (SEM) image of TiB_w/TA15 composites showed a network structure (Fig. 1). The TA15 powder particles were retained during the fabrication process and transformed into prior β grains after sintering, which can be regarded as "soft" units in the network structure. The TiB_w-rich region surrounding the prior β grains formed a spatial network structure, with high strength which can also retain the connectivity of prior β grains.

Figure 2 shows the schematic diagram of hot rolling process. The slabs used for rolling were cut from DRTMCs to dimensions of $200 \text{ mm} \times 240 \text{ mm} \times 15 \text{ mm}$, and each was packed with two pieces of steel sheet (Q235 steel, $240 \text{ mm} \times 300 \text{ mm} \times 6 \text{ mm}$). The packed slabs were used for

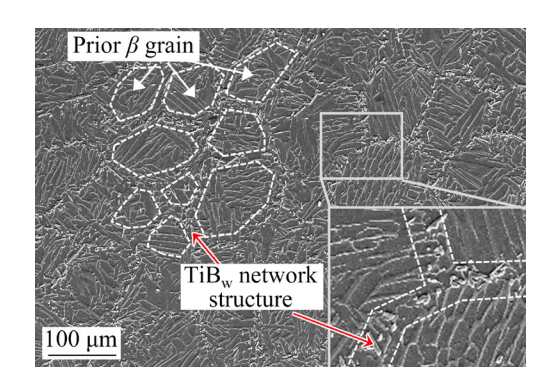


Fig. 1 SEM image of TiB_w/TA15 composites with network structure

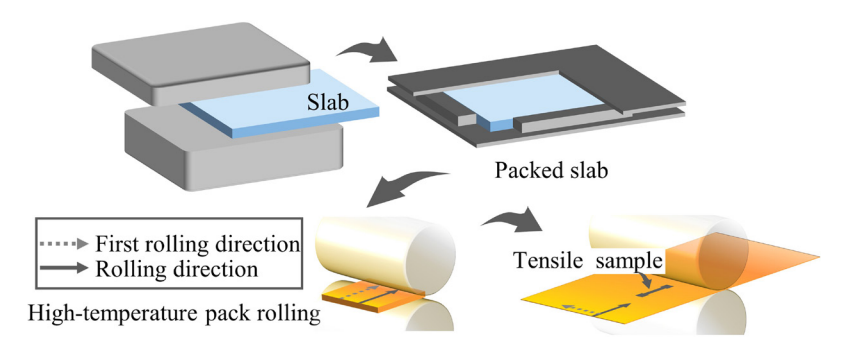


Fig. 2 Schematic diagram of hot rolling process

hot rolling. During the whole rolling process, the packed slab was heated to the target temperature three times (heat preservation for 30 min each time). After each heating step, the slab was continuously rolled three times. The rolled sheet was then cooled to room temperature in air. To reduce the anisotropy of the rolled sheet, the rolling direction was changed three times during the whole process. The first RD of the sheet was perpendicular to the main extension direction (RD). The temperature conditions selected for the rolling preheating were 1000 and 1100 °C, respectively, under which the fine formability of the DRTMCs was observed.

SEM (ZEISS SUPRA 55) was used to study the microstructural and fracture surfaces. Kroll's solution (5 vol.% HF + 15 vol.% HNO₃ + 85 vol.% H₂O) was utilized for etching the polished samples. The crystal structures were analyzed by electron backscattering diffraction (EBSD) tool equipped with CHANNEL 5 software. Dog-bone shaped tensile samples were used for tensile testing. Due to different thicknesses of the sheets rolled at two temperatures, the tensile samples also showed two varied thicknesses. The parallel part dimensions of the samples used in room-temperature tensile testing were $45 \text{ mm} \times 15 \text{ mm} \times 1.8 \text{ mm}$ (cut from the sheet rolled at 1000 °C) and 45 mm \times 15 mm \times 1.3 mm (cut from the sheet rolled at 1100 °C). The parallel part dimensions of the samples used in high-temperature tensile testing were 15 mm × $2 \text{ mm} \times 1.8 \text{ mm}$ and $15 \text{ mm} \times 2 \text{ mm} \times 1.3 \text{ mm}$. All tensile samples were cut along the RD of the sheet.

The high-temperature tensile properties were tested on an Instron-5500R testing machine with a cross-head speed of 1 mm/min. Three tensile samples were tested under each tensile condition.

3 Results and discussion

3.1 Size and surface quality of TMCs rolled sheets

Good formability of DRTMCs at the rolling temperature led to the formation of two TiB_w/TA15-based complete sheets without cracks. The estimated dimensions of sheets rolled at 1000 and 1100 °C were 932 mm \times 393 mm \times 2.0 mm with a reduction rate of 86.7% and 987 mm \times 461 mm \times 1.6 mm with a reduction rate of 89.3%, respectively. This work showed that the adopted temperature conditions and the rolling process were suitable for the preparation of large-sized sheets.

During hot rolling, the slab was deformed with the pack, which protected its surfaces from excessive oxidation. Figure 3 shows the SEM images of the rolled sheet surfaces, with marked surface oxide layers of both sheets. Slight oxidation of the sheets was observed, and the thickness of the oxide layer on the sheet rolled at 1000 °C (12.4 µm, Fig. 3(a)) was thinner than that on the sheet rolled at 1100 °C (27.2 µm, Fig. 3(b)). Thus, the oxidation became severer as the rolling temperature rose.

The near-surface microstructure (RD-TD plane) (TD: transverse direction) of the sheets rolled at both temperatures differed remarkably (Figs. 3(c) and (d)). The evolution of the microstructure during hot rolling is further described below.

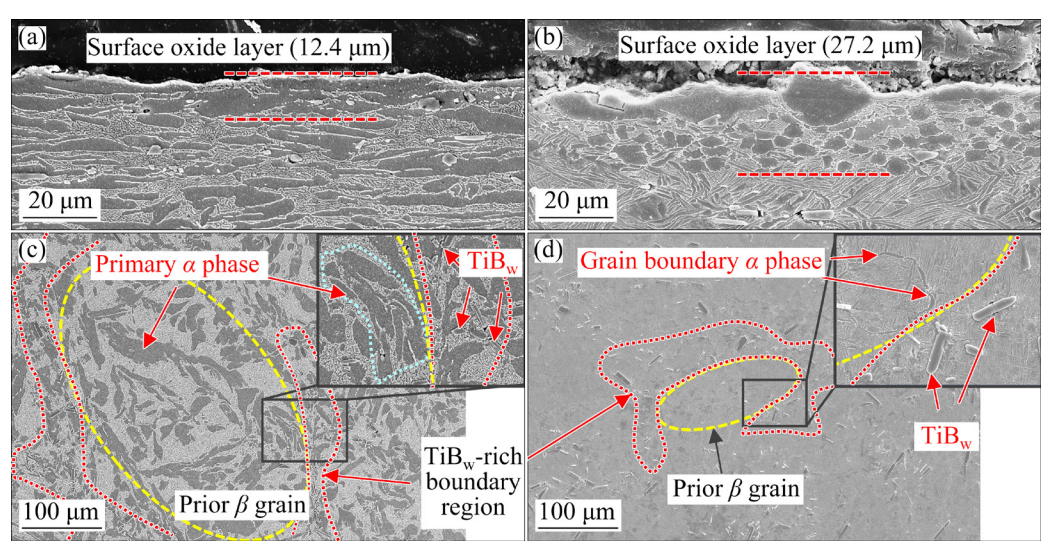


Fig. 3 SEM images showing cross-section (a, b) and surface (c, d) microstructures of sheets rolled at 1000 °C (a, c) and 1100 °C (b, d)

3.2 Microstructural evolution

3.2.1 Microstructure of rolled sheets

Figure 4 displays the microstructures at the thickness center of the sheets in the RD-ND (ND: normal direction) plane. Figures 4(a) and (b) show SEM images of the sheet rolled at 1000 °C at different magnifications, and Figs. 4(c-e) present the SEM images of the sheet rolled at 1100 °C. The characteristics of the microstructure at the center of the sheets were consistent with those near the surface. No excessive growth of β grains or inhomogeneous micro- structures was observed. As reported in literature, TiBw-rich region can impose a pinning effect on the grain boundaries during hightemperature deformation [21], which can enhance the stability of the microstructure. Therefore, DRTMCs with network structure can be deformed at 1100 °C (about 80 °C above transformation temperature from $\alpha + \beta$ to β), which is an inappropriate hot rolling temperature for titanium alloy.

Based on the distribution of TiB_w -rich regions in the microstructure, the prior β grains and network structure of the rolled sheet can be distinguished

roughly. After hot rolling, the slab became seriously thin in the thickness direction, which transformed equiaxed prior β grains in the microstructure ("soft" units in the network structure) into oblate spheroids and reduced the size of the network structure in the ND. The change in the shape of the network structure increased the distribution area and reduced the distribution density of TiB_w , whereas the connectivity between the matrix increased.

During the high-temperature rolling process, TiB whiskers hindered the deformation of the composite, which led to stress concentration in the area near the boundary of TiB_w and matrix. Since stress concentration can be relieved through matrix deformation, most TiB whiskers were unbroken after hot rolling. Several fractured TiB whiskers can be observed in the microstructure (Figs. 4(a) and (c)). The holes appeared at the fracture or on the sides of the TiB_w along the RD as a result of inconsistent deformation between TiB_w and matrix.

3.2.2 Microstructure evolution during hot-rolling process

Figure 5 provides the schematic of the micro-

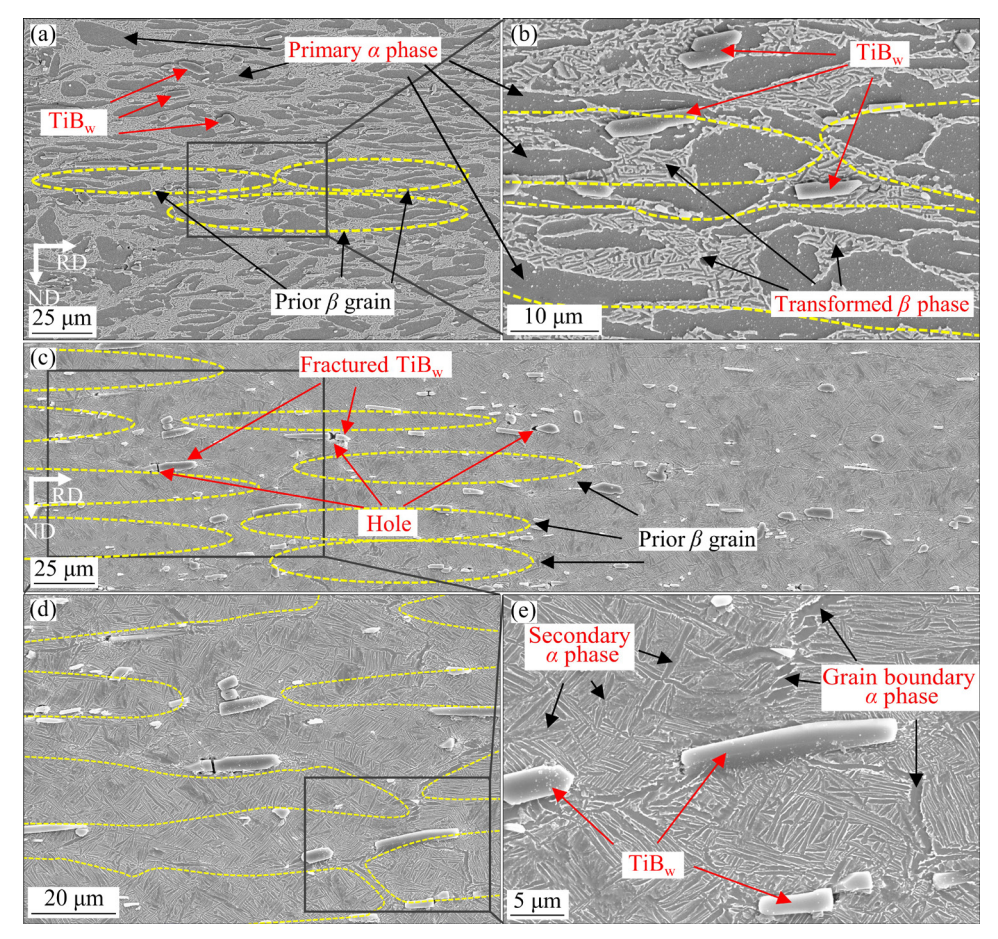


Fig. 4 SEM images showing center of cross-section of sheets rolled at different temperatures: (a, b) 1000 °C; (c-e) 1100 °C

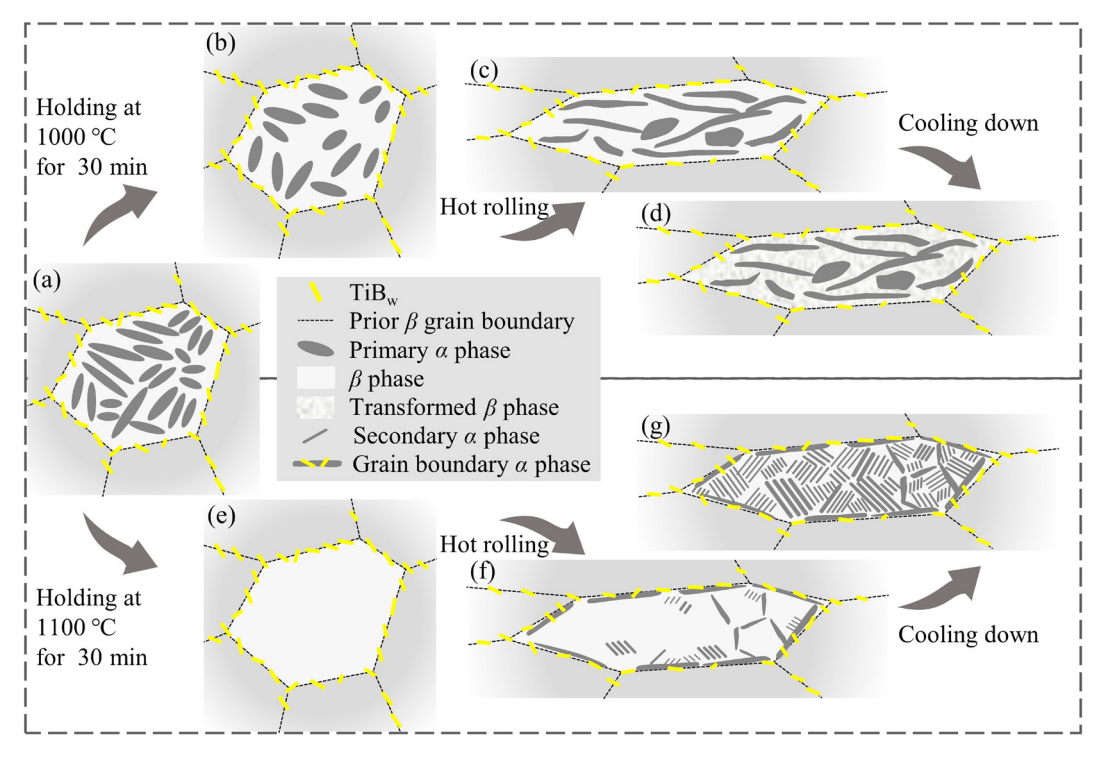


Fig. 5 Schematic of microstructural evolution during hot rolling: (a) Microstructure of slab; (b-d) Sheet rolled at 1000 °C; (e-g) Sheet rolled at 1100 °C

structural evolution during hot rolling. Figure 5(a) represents the slab microstructure, whereas Figs. 5(b-d) show the microstructural evolutions during holding at $1000\,^{\circ}$ C, hot rolling, and air cooling, respectively. The quantity of α phases in the microstructure gradually decreased after maintaining the slab at $1000\,^{\circ}$ C (Fig. 5(b)). In subsequent hot rolling, the α phases became twisted, stretched, or kneaded into blocks (Fig. 5(c)). During the air-cooling process, the short rod-like α phase grew from β phase, turning β phase into transformed β phase (Fig. 5(d)).

Figures 5(e-g) depict the microstructural evolution of sheet rolled at 1100 °C. Given that the holding temperature was considerably higher than the $(\alpha+\beta)/\beta$ transformation temperature (about 1020 °C), the primary α phase was completely transformed into β phase after holding at 1100 °C. During the hot-rolling process, new small β grains were generated by dynamic recrystallization. Figures 3(d) and 4(e) show the boundary α phases generated from the small β grains. The newly formed β grains stopped growing as the temperature of the sheet dropped. In addition, the α phase formed first at the grain boundaries of prior and newly formed β grains (Fig. 5(f)). After further

cooling, the slender secondary α phases formed to fill the whole prior β grains (Fig. 5(g)).

3.2.3 Orientation of grains in rolled sheets

The EBSD data tested at the thickness center of the sheets in the RD–ND plane were used to plot graphs. Figures 6 and 7 display the data of sheets rolled at 1000 and 1100 °C, respectively.

The microstructure of the sheet rolled at 1000 °C mainly consisted of TiBw, transformed β phase, and residual primary α phase. The transformed β phase, which was evolved from the high-temperature β phase during air cooling, consisted of fine α and β phases. In bond contrast (BC) graph, the transformed β phase was shown as a dark area with dense red points (β phase (Fig. 6(a)). In the inverse pole figure (IPF) map of the α phase, the transformed β phase was depicted as the area with small dots of different colors, representing fine α phases with various orientations. The primary α phase was shown as bright blocks and strips in the BC graph. Given that the slab was deformed during hot rolling, the primary α phase strips became twisted and stretched. In the rolled sheet, most strips were arranged along the RD (main extension direction). The orientations of various parts in the same primary α phase exhibited

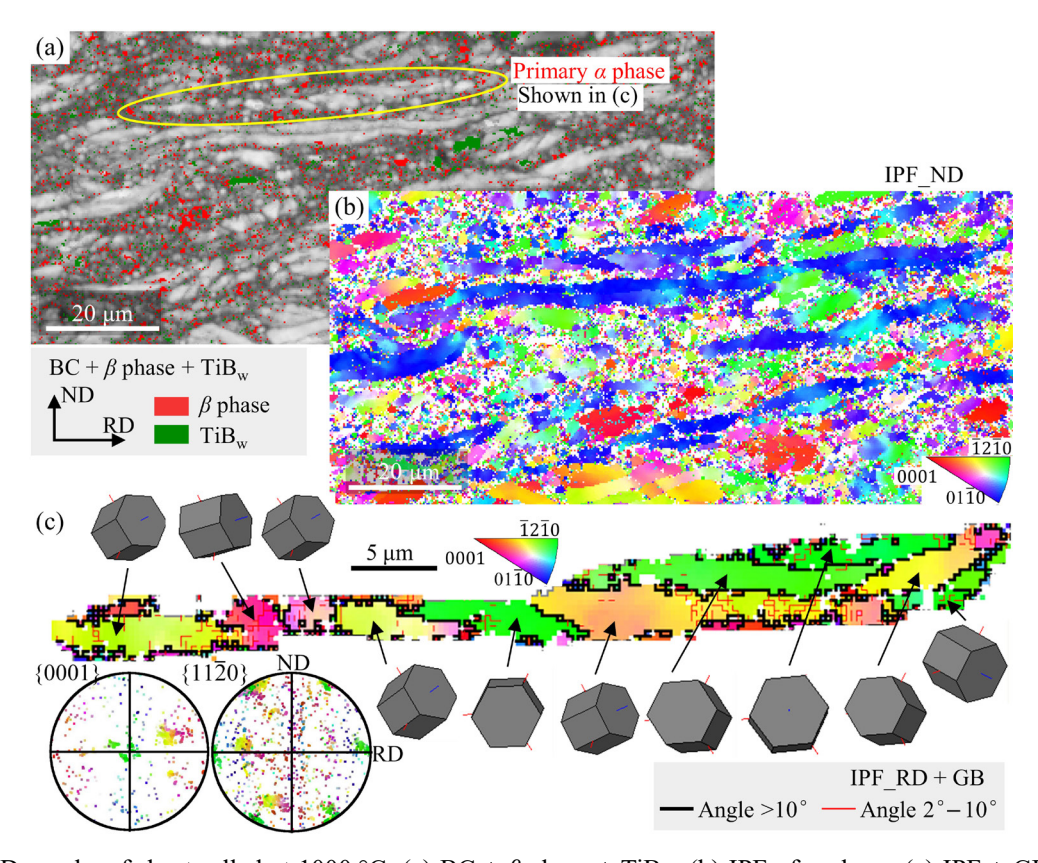


Fig. 6 EBSD graphs of sheet rolled at 1000 °C: (a) BC + β phase + TiB_w; (b) IPF of α phase; (c) IPF + GB and PF of primary α phase

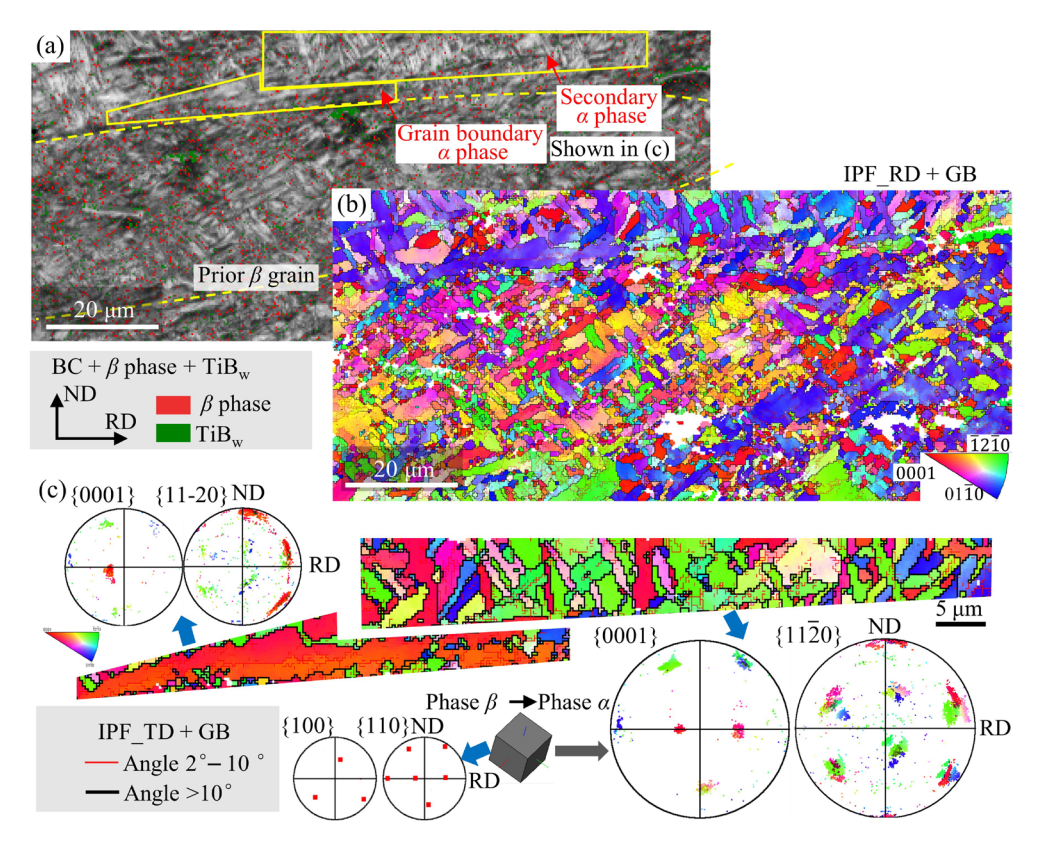


Fig. 7 EBSD graphs of sheet rolled at 1100 °C: (a) BC + β phase + TiB_w phase; (b) IPF + GB of α phase; (c) IPF + GB and PF of α phase

different morphologies, showing an uneven color in the primary α strip in the IPF map (Fig. 6(b)). To analyze the orientation distribution, the single primary α phase marked in Fig. 6(a) was enlarged (Fig. 6(c)). The primary α phase was divided into regions with different colors, representing subgrains with various orientations formed through dynamic recovery. Thus, the points in the pole figure were scattered (Fig. 6(c)).

Before rolling, the microstructure of the slab was completely converted into β phase during holding at 1100 °C. The binding effect of TiB_w kept the grain boundary of β grains on the network structure. During air cooling, the generated β was refilled with grain boundary α phase and secondary α phase. One generated β grain is distinguished and marked in Fig. 7(a). The IPF map of α phase is shown in Fig. 7(b). The secondary α phase and grain boundary α phase near the β grain boundary are also marked. The left selection in Fig. 7(c) shows the marked grain boundary α phase. A minor orientation difference was observed in the grain boundary α phase (pole figure), which indicated the deformation of the grain boundary α phase during rolling. The small-angle grain boundaries formed through dynamic recovery were also found in the IPF map. The right selection in Fig. 7(c) shows the secondary α grains generated from one β grain. During precipitation of α phases from β grains, the $\{0001\}$ crystal planes of the generated α phases were parallel to the $\{110\}$ plane of β phase [27,28], consistent with the pole diagram.

3.2.4 Evolution of network structure

At reduction rates of rolled sheets greater than 85%, the size of the network structure changed seriously. The sheet rolled at 1100 °C was used to describe dimensional changes in the network structure since the network structure in the

microstructure was easy to distinguish through the distribution of TiB_w and grain boundary α phase.

During the hot-rolling process, the network structure remained around the prior β grains ("soft" units), and the size of the network structure can be determined by the size of prior β grains. The outline of prior β grains after hot rolling is marked by a dotted line in Fig. 4(c). The average thickness of flat prior β grains located at the thickness center of the sheet was 13 µm. In the slab microstructure, the average size of relatively complete prior β grains approximated 113 µm. Based on the reduction rate of 89.3%, the average thickness of flat grains was 12.1 µm. The difference in the thickness of the network structure was caused by uneven deformation in the rolled sheets, which commonly occurs during the hot-forming process [15,29-31]. The deformation on the hot-rolled sheet surface was greater than that at the thickness center, leading to larger thickness of the network structure at the center than that on the sheet surface and calculated average thickness. The difference between the calculated thickness of the network structure and the measured thickness was small, indicating a negligible unevenness of the network structure along the thickness direction.

Figure 8 shows the slab deformation in three directions and the evolution of the network structure of the sheet rolled at 1100 °C. The thickness was reduced by 89.3%, and the elongations in RD and TD were 311% and 131%, respectively. As a result of severe thinning, the shape of prior β grains ("soft" units of the network structure) transformed from equiaxed round balls into disk-like ellipsoids (Fig. 8). In addition, the network structure with equiaxed units turned into a layered structure with disk-like units, with the microstructure exhibiting a similar layout structure as multi-layer materials.

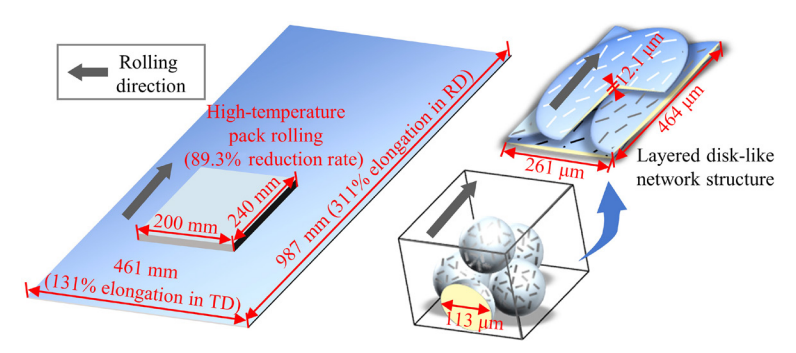


Fig. 8 Diagram showing network structural evolution during hot rolling at 1100 °C

3.3 Mechanical properties of rolled sheets

3.3.1 Tensile strength at room temperature

Figure 9 shows the room-temperature tensile properties of the slab and rolled sheets. The tensile strength of the slab was 1106 MPa, whereas those of sheets rolled at 1000 and 1100 °C were 1398 and 1360 MPa, respectively. Compared to that of the slab, the tensile strengths of the sheets rolled at 1000 and 1100 °C were increased by 26.4% and 23.0%, respectively. As described above, the microstructure of the slab and the size of network structure considerably changed during hot rolling, which would have a complex effect on the tensile strength.

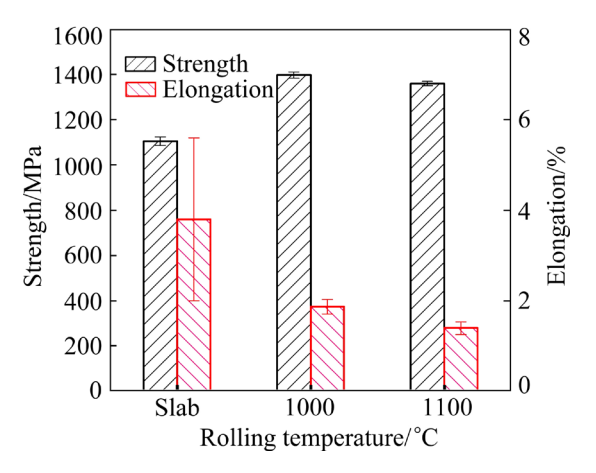


Fig. 9 Tensile strength and elongation of slab and rolled sheets at room temperature

Higher strength of sheets compared with that of the slab can be explained by various factors. The first involved the increased strength of the matrix, which improved the strength of the sheets. After rolling deformation, the microstructure of the matrix in the rolled sheet became denser and was composed of finer grains, which can reduce the risk of failure and improve the resistance to deformation. Secondly, the decrease in the distribution density of TiB_w and thickness of the network structure was conducive for TiB_w to share stress and reduce excessive stress concentration in the network structure during tensile testing. Thirdly, more TiB whiskers were distributed along the RD, indicating a better capability to bear stress [32,33].

Given that the sheets possessed similar network structures, the difference in mechanical properties should have been caused by various microstructures of the matrix. According to literature [34,35], TA15 titanium alloy with primary

 α phases and transformed β structure should have higher room-temperature mechanical strength and elongation than that with strip secondary α phases. Thus, the sheet rolled at 1000 °C possessed better strength and plasticity than that rolled at 1100 °C.

3.3.2 Fracture mechanism of room-temperature tensile specimens

The rolled sheets showed brittle fractures in room-temperature tensile testing with very small plastic deformation. After a crack initiates on the surface or at a defect, it quickly propagates through the cross-section of the material, leading to the fracture. During the whole fracture process, the propagation speed of the crack increases as the crack area enlarges, resulting in a faster crack extension and a rougher fracture surface.

Figure 10 shows the macro photographs and SEM images of the fracture planes of the tested tensile specimens. Figures 10(a-c) present the fracture plane of the sheet rolled at 1000 °C, whereas Figs. 10(d-g) depict the fracture plane of the sheet rolled at 1100 °C. Among the images, Figs. 10(a) and (d) are macro photographs.

The characteristics of brittle fractures, including evident crack source, smooth region, radial region, and shear lips, were visible in the fracture planes (Fig. 10(e)). In the early stage of fracture, the area of the main crack was small. In addition, the stress caused by the crack tip was low, under which the crack slowly expanded and formed a smooth region. The smooth area of the whole fracture plane is marked in Figs. 10(a) and (e).

As the main crack grew, the stress caused by the crack tip increased, and more areas near the crack tip were affected. Microcracks appeared in the stress-affected area and likely connected with the crack tip of the main crack from different directions. Therefore, the shape of the crack tip became more tortuous, and radial patterns remained after the crack tip fast passed. In this fracture stage, stress concentration occurred around TiBw, leading to the fracture of TiBw. Microcrack formed in the broken $TiB_{\rm w}$ and expanded toward other broken TiBwhiskers. After the connection of microcracks with the main crack, large numbers of broken TiB whiskers were found in the fracture plan. Given that the TiB-rich areas in the rolled sheet were around the "soft" units, after the main crack passed through these areas, hollows and bulges were shown in the fracture plan.

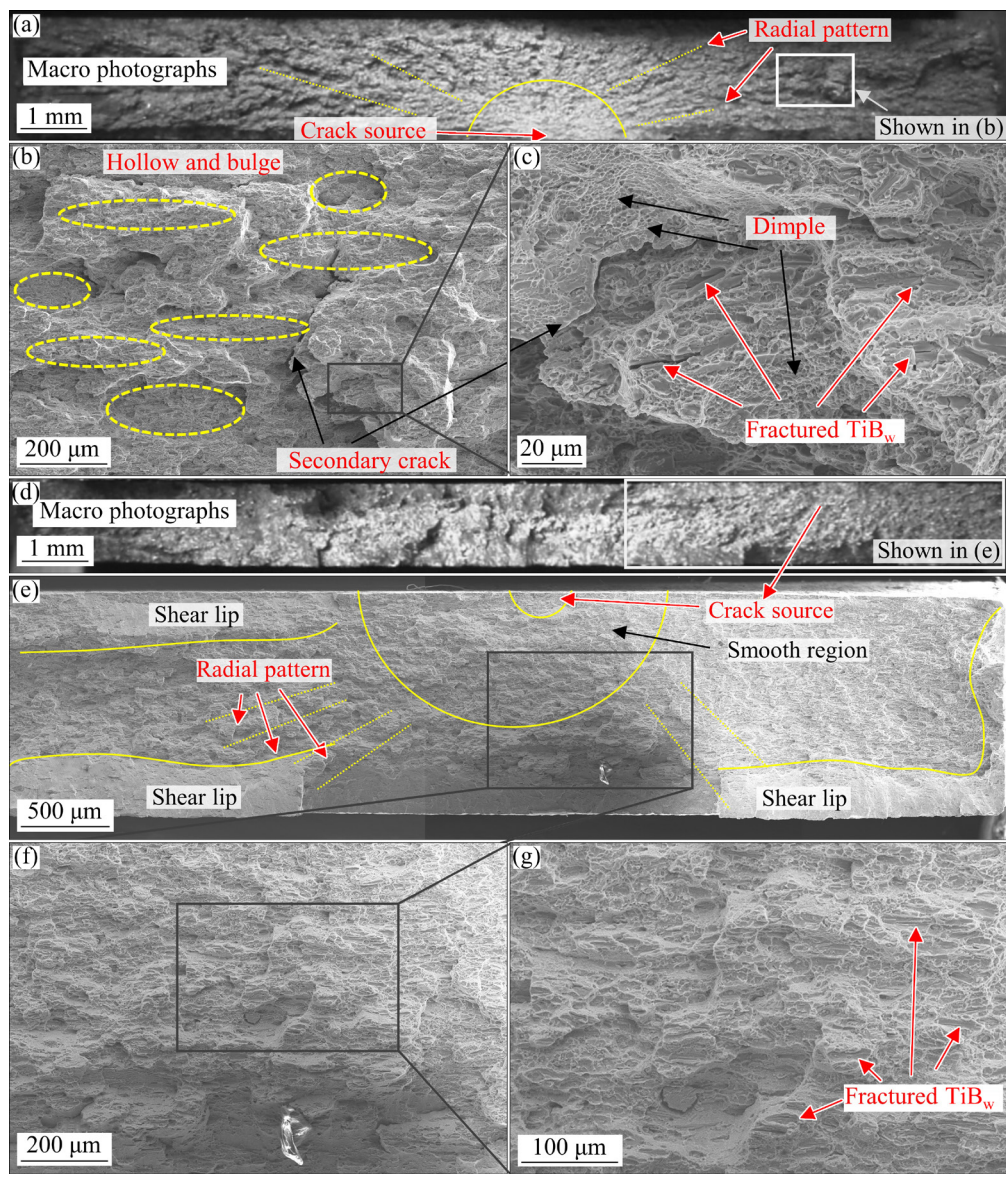


Fig. 10 Macro photographs (a, d) and SEM images (b, c, e–g) of fracture planes: (a–c) Fracture planes rolled at 1000 °C; (d–g) Fracture planes rolled at 1100 °C

In the last stage of fracture, multiple secondary cracks expanded simultaneously and intersected to form the main crack. The latter passed through the specimen instantaneously to form large-sized peaks or valleys. After cracks passed through the specimen, the plastic deformation of the matrix created numerous tiny dimples. Almost all TiB whiskers shown in the fracture plane were broken and fully played reinforcing roles [15]. Moreover, no difference was observed in the fracture mechanisms between the sheets rolled at 1000 and 1100 °C.

3.3.3 Tensile strength at high temperatures

The elongations of the slab and sheets tested at 600 °C were 4.7% (slab), 14.9% (rolled at 1000 °C), and 12.6% (rolled at 1100 °C) (Fig. 11). The

plasticity of the sheets was improved compared with that of the slab tested at room temperature, mainly because of the improved plasticity of the matrix. The transformed β phase consisted of fine grains and was prone to deformation at high temperatures. Thus, the sheet rolled at $1000\,^{\circ}\text{C}$ showed the best plasticity among sheets and slab, consistent with tensile test results at 650 and 700 °C (Fig. 11(b)).

The tensile strengths of the slab and sheets tested at 600 °C were 561 (slab), 662 (rolled at 1000 °C), and 758 MPa (rolled at 1100 °C). The higher strength of sheets compared with that of the slab was caused by the change in the size of network structure. After rolling, the area of network

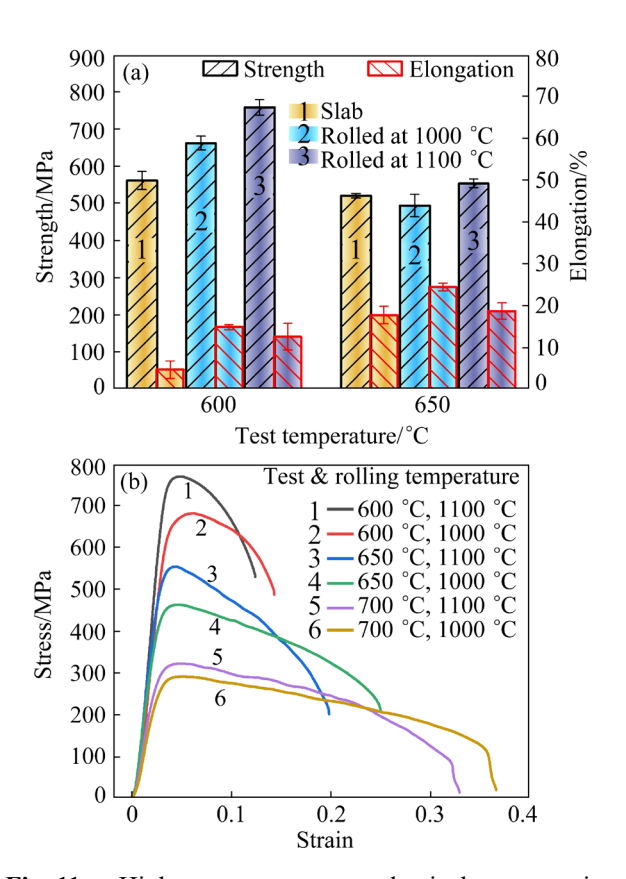


Fig. 11 High-temperature mechanical properties: (a) Tensile strength and elongation of slab and rolled sheets tested at 600 and 650 °C; (b) Stress–strain curves of sheets tested at 600, 650, and 700 °C

structure in the rolled sheet increased, thereby reducing the density of TiB whiskers. The proper dispersion of TiB_w can also reduce stress concentration in the network structure and prevent premature failure. The matrix with elongated α phase has higher high-temperature deformation resistance [36]; therefore, the high-temperature tensile strength of the sheet rolled at 1100 °C was higher than that rolled at 1000 °C. This outcome was also reflected in the results of tensile tests at 650 and 700 °C (Fig. 11(b)).

The tensile strengths of the slab and rolled sheets at 650 °C were 521 MPa (slab with elongation of 17.7%), 494 MPa (rolled at 1000 °C with elongation of 24.5%), and 553 MPa (rolled at 1100 °C with elongation of 18.7%). The mechanical properties of the slab and rolled sheets were similar at 650 °C. During the tensile process, given the greatly reduced strength of the matrix, the stress concentration near the TiB whisker can tear the matrix material and produce holes. The generated and enlarged holes continuously relieved the stress

concentration, and the stress acting on TiB whiskers can no longer break them. Therefore, the strengthening effect of TiB whiskers was seriously weakened. In other words, the tensile strength of the sheets largely depended on the strength of the matrix during tensile tests at 650 °C. The tensile strengths of the rolled sheets and the differences between them further decreased in the tensile tests at 700 °C (Fig. 11(b)).

3.3.4 Fracture mechanism of high-temperature tensile specimens

The fracture morphologies of the rolled sheets in the tensile tests at the same temperature were almost the same. Thus, the tensile specimens of the sheets rolled at 1100 °C were studied at 600 and 650 °C. During the high-temperature tensile fracture process, the material underwent a significant degree of plastic deformation. Hole defects were easily generated near the reinforcing particles in the material, and cracks tended to propagate along these defect-dense areas.

Figures 12(a, c, e, g, i) show the SEM images of tensile samples tested at 600 °C, whereas Figs. 12(b, d, f, h, j) illustrate those tested at 650 °C. Figs. 12(a-f) show the fracture planes, and Figs. 12(g-j) depict the microstructures of the sample surface near the fracture.

The comparison of fracture morphologies in Figs. 12(a) and (b) revealed sharp steps in fractures of the samples tested at 600 °C, and they were caused by rapid intersections of microcracks in a large space area. The steps of the sample tested at 650 °C appeared gentle, indicating a small stress concentration at the crack tip, and the expansion of the microcrack was accompanied by evident plastic deformation. Large-sized dimples existed on the fracture of the sample tested at 650 °C, and they were caused by a large plastic deformation before fracture.

Broken TiB whiskers damaged by stress concentration were found at the tips and roots of the steps in the fracture of the sample tested at 600 °C (Fig. 12(c)), and this finding suggested that TiB_w still undertook the stress and played a good strengthening effect. For the fracture of the sample tested at 650 °C (Fig. 12(d)), a large number of complete TiB whiskers were found at the center of dimples, which was due to the stress concentration near TiB_w deformed the matrix without causing the fracture of TiB_w.

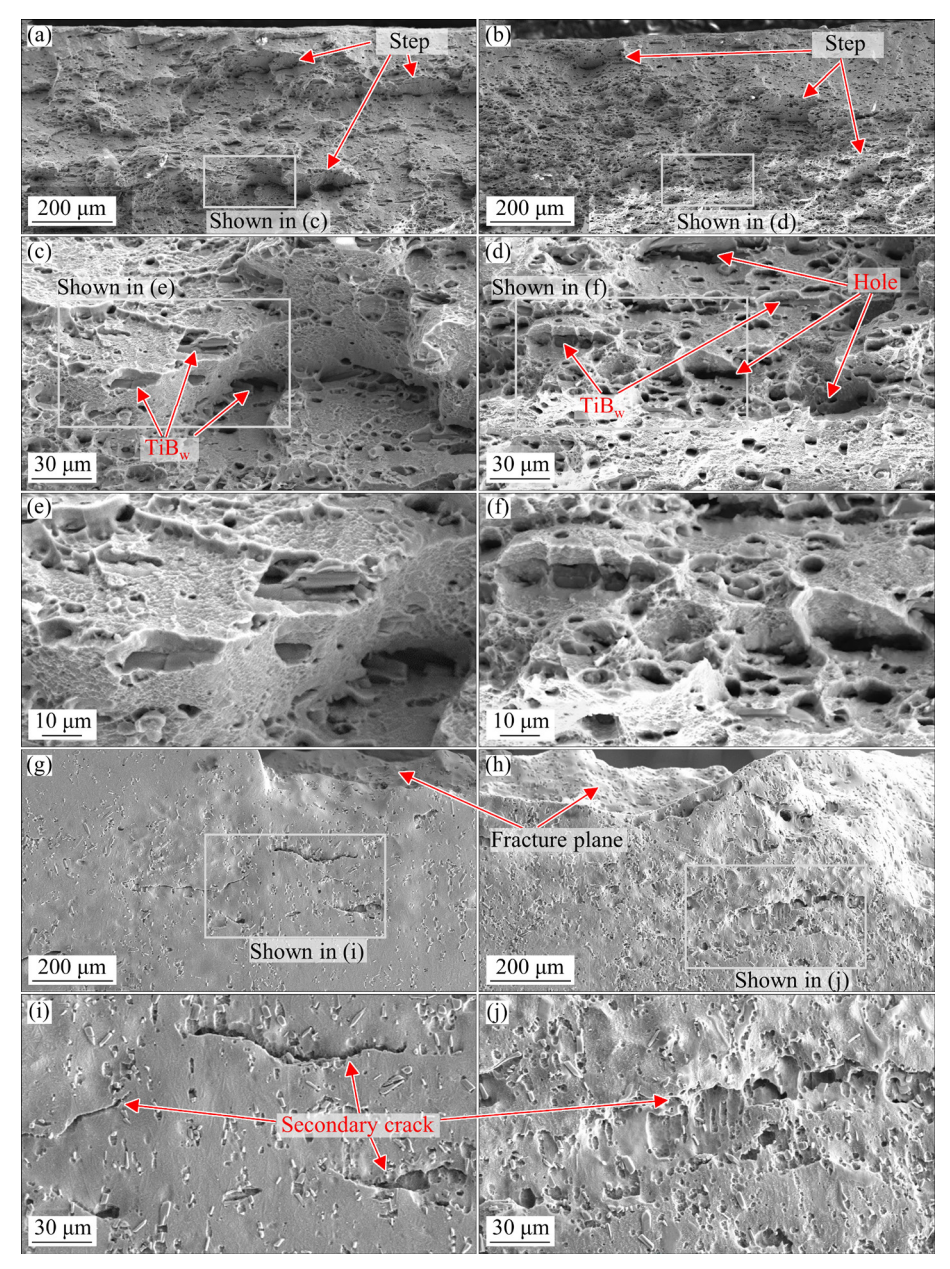


Fig. 12 SEM images of fracture planes (a-f) and surfaces (g-j) of samples tested at 600 °C (a, c, e, g, i) and 650 °C (b, d, f, h, j)

Secondary cracks were found in the sample surface near the fracture (Figs. 12(g) and (h)). The secondary cracks had a sharp shape in the sample tested at 600 °C, consistent with the fracture morphology. For the sample tested at 650 °C, the material on both sides of the crack has undergone significant plastic deformation, and long strip holes were left beside TiB_w, showing the state of crack expansion in a good plasticity matrix.

4 Conclusions

(1) The microstructures of the rolled sheets

were uniform and without excessively grown β grains. The microstructures formed during heat preservation at 1000 and 1100 °C before rolling were different, which led to varied microstructures of the rolled sheets. After rolling deformation, the network structure with equiaxed units was turned into a layered structure with disk-like units.

(2) The rolled sheets were subjected to fracture with brittleness during room-temperature tensile testing. The sheet rolled at 1000 °C displayed better room-temperature strength and elongation than that rolled at 1100 °C. Compared with slabs, the tensile strengths of the sheets rolled at 1000 and 1100 °C

688 - 692.

increased by 26.4% (1398 MPa) and 23.0% (1360 MPa), respectively.

- (3) The sheet rolled at 1000 °C had the best plasticity, whereas that rolled at 1100 °C had the best strength. During the tensile test at 600 °C, the TiB whiskers maintained a good strengthening effect. The tensile strengths of the slab and sheets were 561 MPa (slab), 662 MPa (rolled at 1000 °C), and 758 MPa (rolled at 1100 °C).
- (4) When the temperature was higher than 650 °C, the tensile strength of the sheets largely depended on the titanium matrix. The tensile strength at 650 °C of the sheet rolled at 1100 °C (553 MPa) was higher than those of the slab (521 MPa) and sheet rolled at 1000 °C (494 MPa).

References

- [1] TJONG S C, MAI Y W. Processing-structure-property aspects of particulate- and whisker-reinforced titanium matrix composites [J]. Composites Science and Technology, 2008, 68: 583-601.
- [2] GORSSE S, MIRACLE D B. Mechanical properties of Ti-6Al-4V/TiB composites with randomly oriented and aligned TiB reinforcements [J]. Acta Materialia, 2003, 51: 2427-2442.
- [3] YANG J H, XIAO S L, CHEN Y Y, XU L J, WANG X P, ZHANG D D. The tensile and fracture toughness properties of a (TiB_w+TiC_p)/Ti-3.5Al-5Mo-6V-3Cr-2Sn-0.5Fe composites after heat treatment [J]. Materials Science and Engineering A, 2018, 729: 21-28.
- [4] DEGNAH A, DU J, RAVI CHANDRAN K S. CALPHAD approach and processing of a multicomponent titanium matrix composite for high strength and fracture toughness [J]. Materials Science and Engineering A, 2020, 781: 139210.
- [5] ZHANG R, HUANG L J, ZHAO X M, GENG L, WANG S, JIANG S L, JIAO Y. Influence of deformation parameters and network structure to the microstructure evolution and flow stress of TiBw/Ti64 composite [J]. Materials Science and Engineering A, 2021: 809.
- [6] HASHIN Z, SHTRIKMAN S. A variational approach to the theory of the elastic behaviour of multiphase materials [J]. Journal of the Mechanics and Physics of Solids, 1963, 11: 127–140.
- [7] HUANG L J, GENG L, PENG H X. Microstructurally inhomogeneous composites: Is a homogeneous reinforcement distribution optimal? [J]. Progress in Materials Science, 2015, 71: 93–168.
- [8] HUANG L J, GENG L, PENG H X, ZHANG J. Room temperature tensile fracture characteristics of in situ TiBw/ Ti₆Al₄V composites with a quasi-continuous network architecture [J]. Scripta Materialia, 2011, 64: 844–847.
- [9] HUANG L J, GENG L, PENG H X, KAVEENDRAN B. High temperature tensile properties of in situ TiB_w/Ti₆Al₄V composites with a novel network reinforcement architecture [J]. Materials Science and Engineering A, 2012, 534:

- [10] JIAO Y, HUANG L J, GENG L. Progress on discontinuously reinforced titanium matrix composites [J]. Journal of Alloys and Compounds, 2018, 767: 1196–1215.
- [11] HUANG L J, AN Q, GENG L, WANG S, JIANG S L, CUI X, ZHANG R, SUN F, JIAO Y, CHEN X, WANG C Y. Multiscale architecture and superior high-temperature performance of discontinuously reinforced titanium matrix composites [J]. Advanced Materials, 2021, 33: 2000688.
- [12] JIAO X Y, CHEN W Z, YANG J L, ZHANG W C, WANG G F. Microstructure evolution and high-temperature tensile behavior of the powder extruded 2.5 vol.% TiB_w/TA15 composites [J]. Materials Science and Engineering A, 2019, 745: 353–359.
- [13] WANG D J, ZHANG R, LIN Z Q, LI H, LIU G, YUAN S J. Effect of microstructure on mechanical properties of net-structured TiB_w/TA15 composite subjected to hot plastic deformation [J]. Composites (Part B): Engineering, 2020, 187: 107798.
- [14] ZHAO E T, SUN S C, YU J R, AN Y K, CHEN W Z, CHEN R R. Dynamic recrystallization and silicide precipitation behavior of titanium matrix composites under different strains [J]. Transactions of Nonferrous Metals Society of China, 2021, 31: 3416–3427.
- [15] FENG Y J, HOU J B, GAO L, CUI G R, ZHANG W C. Research on the inhomogeneity and joint interface of in situ oriented TiB_w/TA15 composites fabricated by vacuum hot-pressing sintering and canned extrusion [J]. Journal of Manufacturing Processes, 2020, 59: 791–800.
- [16] FENG Y J, CUI G R, ZHANG W C, CHEN W Z, YU Y. High temperature tensile fracture characteristics of the oriented TiB whisker reinforced TA15 matrix composites fabricated by pre-sintering and canned extrusion [J]. Journal of Alloys and Compounds, 2018, 738: 164–172.
- [17] WANG S, AN Q, ZHANG R, JIANG S, HUANG L J, CHEN R, LIU B X, JIAO Y, GENG L. Microstructure characteristics and enhanced properties of network-structured TiB/(TA15-Si) composites via rolling deformation at different temperatures [J]. Materials Science and Engineering A, 2022, 829: 142176.
- [18] ZHANG R, WANG D, YUAN S. Effect of multi-directional forging on the microstructure and mechanical properties of TiB_w/TA15 composite with network architecture [J]. Materials & Design, 2017, 134: 250–258.
- [19] FENG Y J, ZHANG W C, CUI G R, WU J P, CHEN W Z. Effects of the extrusion temperature on the microstructure and mechanical properties of TiB_w/Ti6A14V composites fabricated by pre-sintering and canned extrusion [J]. Journal of Alloys and Compounds, 2017, 721: 383–391.
- [20] YU Y, ZHANG W C, DONG W Q, YANG J L, FENG Y J. Effects of pre-sintering on microstructure and properties of TiBw/ Ti6Al4V composites fabricated by hot extrusion with steel cup [J]. Materials Science and Engineering A, 2015, 638: 38–45.
- [21] ZHANG W C, FENG Y J, CHEN W Z, YANG J. Effects of heat treatment on the microstructure and mechanical properties of in situ inhomogeneous TiB_w/Ti₆Al₄V composite fabricated by pre-sintering and canned powder extrusion [J]. Journal of Alloys and Compounds, 2017, 693: 1116–1123.

- [22] WANG S, HUANG L J, JIANG S, ZHANG R, SUN F B, AN Q, GENG L. Multiplied bending ductility and toughness of titanium matrix composites by laminated structure manipulation [J]. Materials & Design, 2021, 197: 109237.
- [23] SHEKHAR A, KUMAR S, ORAON M, ROY M K Revisiting the rolling process and its future research potentials [J]. AIP Conference Proceedings, 2020, 2273: 050031.
- [24] PUSTOVOYTOV D, PESIN A, TANDON P. Asymmetric (hot, warm, cold, cryo) rolling of light alloys: A Review [J]. Metals, 2021, 11: 956.
- [25] ZHOU Y, YANG F, CHEN C G, SHAO Y R, LU B X, SUI Y L, GUO Z M. Mechanical property and microstructure of in-situ TiB/Ti composites via vacuum sintering and hot rolling [J]. Journal of Alloys and Compounds, 2022, 911: 165042.
- [26] JIAO Y, HUANG L J, AN Q, JIANG S, GAO Y N, CUI X P, GENG L. Effects of Ti₅Si₃ characteristics adjustment on microstructure and tensile properties of in-situ (Ti₅Si₃ + TiB_w)/Ti₆Al₄V composites with two-scale network architecture [J]. Materials Science and Engineering A, 2016, 673: 595–605.
- [27] BHATTACHARYYA D, VISWANATHAN G B, DENKENBERGER R, FURRER D, FRASER H L. The role of crystallographic and geometrical relationships between α and β phases in an α/β titanium alloy [J]. Acta Materialia, 2003, 51: 4679–4691.
- [28] OBASI G C, BIROSCA S, FONSECA J Q D, PREUSS M. Effect of β grain growth on variant selection and texture memory effect during $\alpha \rightarrow \beta \rightarrow \alpha$ phase transformation in Ti-6Al-4V [J]. Acta Materialia, 2012, 60: 1048–1058.
- [29] CHEN X, CAI Q W, XIE B S, YUN Y, ZHOU Z Y.

- Simulation of microstructure evolution in ultra-heavy plates rolling process based on Abaqus secondary development [J]. Steel Research International, 2018, 89: 1800409.
- [30] XIE B S, CAI Q W, YUN Y, LI G S, NING Z. Development of high strength ultra-heavy plate processed with gradient temperature rolling, intercritical quenching and tempering [J]. Materials Science and Engineering A, 2017, 680: 454–468.
- [31] YU W, LI G, CAI Q. Q345 ultra-heavy plate rolled with temperature gradient [J]. Materials and Manufacturing Processes, 2015, 30: 104–110.
- [32] GUO X L, WANG L Q, WANG M M, QIN J W, ZHANG D, LU W J. Effects of degree of deformation on the microstructure, mechanical properties and texture of hybrid-reinforced titanium matrix composites [J]. Acta Materialia, 2012, 60: 2656–2667.
- [33] HUANG L J, GENG L, WANG B, XU H Y, KAVEENDRAN B. Effects of extrusion and heat treatment on the microstructure and tensile properties of in situ TiB_w/Ti₆Al₄V composite with a network architecture [J]. Composites (Part A): Applied Science and Manufacturing, 2012, 43: 486–491.
- [34] LU J, WANG Y H, ZHANG W F. Effect of microstructure on tensile properties of near-alpha TA15 titanium alloy [J]. Heat Treatment of Metals, 2011, 36: 25–28. (in Chinese)
- [35] ARAB A, CHEN P W, GUO Y S. Effects of microstructure on the dynamic properties of TA15 titanium alloy [J]. Mechanics of Materials, 2019, 137: 103121.
- [36] XU L J, ZHENG Y F, LIANG Z Q, HAN S W, XUE X, XIAO S L, TIAN J, CHEN Y Y. Creep behavior and microstructure evolution of titanium matrix composites reinforced with TiB, TiC and Y₂O₃ [J]. Transactions of Nonferrous Metals Society of China, 2023, 33: 467–480.

网状结构 TiB_w/TA15 复合材料热轧薄板的 显微组织演变与力学性能

钱健行1, 王克环1, 曾元松2, 付明杰2, 王富鑫2, 刘 钢1

- 1. 哈尔滨工业大学 材料科学与工程学院,哈尔滨 150001;
 - 2. 中国航空制造技术研究院,北京 100024

摘 要:通过包套热轧方法,在 1000 和 1100 ℃温度下热轧制备两张具有网状结构 TiBw/TA15 钛基复合材料薄板。两张薄板的轧下率分别为 86.7% (尺寸为 932 mm×393 mm)和 89.3% (尺寸为 987 mm×461 mm)。两张热轧薄板的显微组织具有显著差异,薄板中的网状结构变成了具有扁平椭球单元的层状结构。相较于板坯,在 1000 和 1100 ℃条件下热轧薄板的室温拉伸强度分别提高了 26.4% (1398 MPa)和 23.0% (1360 MPa)。在 600 ℃拉伸试验中板坯和薄板的抗拉强度为 561 MPa(板坯)、662 MPa (1000 ℃热轧薄板)和 758 MPa (1100 ℃热轧薄板)。在 650 ℃的拉伸试验中,1100 ℃热轧薄板的抗拉强度(553 MPa)最高。

关键词: 钛基复合材料; 网状结构; 热轧; 薄板; 力学性能; 断裂分析